Morphological study of the structure developed during the polymerization of a series of segmented polyurethanes

A. L. Chang, R. M. Briber and E. L. Thomas
Polymer Science and Engineering Department, University of Massachusetts, Amherst, Massachusetts 01003, *USA*

and R. J. Zdrahala and F. E. Critchfield
Union Carbide Corporation, South Charlestown Technical Center, South Charlestown, West Virginia 25303, *USA*
(*Received* 4 *April* 1981; *revised* 22 *September* 1981)

The morphology developed during the polymerization of a series of linear polyurethanes ranging from 10–77% by wt. hard segment has been characterized by a variety of techniques. The polyurethanes were batch reacted using poly(propylene oxide) endcapped with poly(ethylene oxide) as the polyol, 4,4'-diphenylmethane diisocyanate and 1,4-butanediol. Hard segment-rich globules and two types of hard segment spherulites have been observed. The size and number of these microstructures depends on cross-sectional location in the mould and hard segment content. A possible polymerization scheme to account for the complex sample morphology is discussed. The importance of these structures on the mechanical properties is illustrated.

Keywords Polyurethane; segmented copolymer; electron microscopy; morphology; microstructure

INTRODUCTION

Most previous work[1-7] on microstructure–property relations for polyurethanes has concentrated on the nature of the hard segment and soft segment microphase separation. While spherulitic superstructure has been occasionally observed for crystalline hard segment materials[8-13], most authors have sought to interpret physical property data in terms of microdomains.

In particular, the extension of the plateau shear modulus to higher temperatures is thought to arise from the physical crosslinking effect of the hard segment domains. In a previous paper we pointed out the existence of several scales of heterogeneities as well as significant skin/core regions occurring in a reaction injection moulded (*RIM*) polyurethane[13]. Because of the fast exothermic urethane reaction, large temperature gradients occur across the mould, resulting in distinctly different skin region/core region microstructures. Two scales of structural organization were observed: (i) of the order of tens of μm, corresponding to hard segment-rich globules (*HSG*) and hard segment-rich spherulites (*HSS*) and (ii) of the order of 100 Å, associated with hard segment-rich fibrils (*HSF*).

The globules, a new morphological feature in polyurethanes, were present near the mould surface and were proposed to be pockets of glassy hard segment-rich material which was unable to crystallize due to low temperature.

As part of an effort to understand better *RIM* polyurethanes, a series of ethylene oxide endcapped poly(propylene oxide)–polyol/4,4'-diphenylmethane diisocyanate/1,4-butanediol (PPO–EO/MDI/BDO) polyurethanes (ranging from 10–77% by wt. hard segment) were prepared by a hand cast procedure. The polyol was endcapped with poly(ethylene oxide) to assure that the reactive ends were primary hydroxyls. An initial study[14] of tensile and dynamic mechanical properties of this system indicated a change from a soft elastomer (continuous soft phase) to a higher modulus plastic (continuous hard phase) at about 55% hard segment content.

Since the catalyst levels used were lower than in *RIM*, the samples were cured in the mould at 100°C for 16 h. A non-crystallizable soft segment was chosen in order to isolate crystallinity to the hard segment phase. To the unaided eye, samples containing up to 55% hard segment appeared uniform while samples having 66 and 77% hard segment content had a distinct cross-sectional variation. The 66 and 77% hard segment content samples were clear in the centre and opaque at the edges, near the mould wall. Detailed optical and electron microscopy studies revealed that all the samples were micro-heterogeneous, consisting of a variety of structures depending on hard segment content and cross-sectional location.

The present work describes these structures and suggests possible reasons for their development. The influence of these large scale structures on the mechanical properties of polyurethanes is illustrated.

EXPERIMENTAL

Materials

The polyurethanes investigated were based on a three-component system that was batch reacted in the mould.

0032-3861/82/071060-09$03.00

Table 1 Summary of composition and heats of fusion for the as-reacted polyurethane system

Sample designation	PPO–EO/MDI/BDO mole ratio	Vol. fraction initial mix PPO–EO/MDI/BDO	Wt. % hard segment	Heat of fusion (cal g^{-1})	
				Polymer	Hard segment
I	1/1.7/0.7	0.80/0.17/0.03	10	~0	~0
II	1/2.8/1.8	0.70/0.24/0.06	21	2.4	11.3
III	1/4.2/3.2	0.60/0.31/0.09	32	3.8	11.7
IV	1/6.1/5.1	0.50/0.38/0.12	43	6.0	13.7
V	1/9.1/8.1	0.40/0.45/0.15	55	10.2	18.5
VI	1/14.0/13.0	0.30/0.52/0.18	66	9.4	14.2
VII	1/23.8/22.8	0.20/0.59/0.21	77	8.8	11.4

The components used were: (i) 4,4'-diphenyl methane diisocyanate (MDI); (ii) poly(propylene oxide) endcapped with 30% ethylene oxide, functionality of 1.96 and $M_n = 2000$ (PPO–EO); and (iii) 1,4-butanediol (BDO).

The batch reaction process was as follows[14]:

(1) Stoichiometric amounts of PPO–EO, vacuum distilled BDO (both dried over molecular sieves) and dibutyltin dilaurate (0.02 wt% based on total polyol and diol weight) were charged into a 500 ml reaction vessel and degassed for 30 min at 60°C. The vacuum was broken and a 4% molar excess over the stochiometric amount of filtered, moulton MDI at 60°C was added. This mixture was stirred at 2500 rpm and degassed for 30 s. The reaction mixture was then poured into a preheated 3.2 mm thick plate glass mould and placed in an oven at 100°C for 16 h. Seven polyurethanes with hard segment concentrations ranging from 10–77% were produced (*Table 1*).

Differential scanning calorimetry (d.s.c.)

A Perkin–Elmer DSC-II was used to characterize the thermal properties of the samples. The temperature scale and energy input of the d.s.c. were calibrated using the melting transition and heat of fusion of an Indium standard. D.s.c. scans of all samples were carried out starting from ambient temperature at a heating rate of 20°C min^{-1} and range of 5 mcal s^{-1}. The sample size was approximately 10 mg. All d.s.c. scans are first scans. Second scans have been previously published by Zdrahala *et al.*[14]. In order to examine the skin/core effect found in the samples of high hard segment content, skin and core portions of samples VI and VII were also run separately. The skin portion was removed with a razor blade by slicing parallel to the surface of the sample to a depth of 0.2 to 0.4 mm.

Cryo ultramicrotomy

The only method available to examine the morphology that developed during the reaction is microtomy. Microscopy then reveals the unpreturbed morphology. A Sorvall MT2-B Porter–Blum ultramicrotome with a low temperature attachment and diamond knife was used. All microtoming was done in the temperature range of −60° to −70°C. Both dry knife and wet knife techniques, where the knife trough is filled with isopropyl alcohol for floating off sections, were used. Thin sections, less than 2000 Å thick, were picked up with 300 or 400 mesh copper grids for electron microscopy.

Electron microscopy

A JEOL 100 CX transmission electron microscope (*TEM*) was operated at 100 kV with magnifications of 2000 to 5000X. Microtomed specimens were directly observed on copper grids of 300 or 400 mesh without support film. Sample mass loss was observed even at low electron doses. Separate studies[15] on pure MDI/BDO and PPO–EO/MDI copolymers indicates the hard segment is relatively radiation resistant while the soft segment degrades.

Scanning electron microscopy (*SEM*) of mechanically-deformed samples was carried out on a ETEC U-1 at 20 kV. Samples were sputter coated with approximately 300 Å of gold.

Wide-angle X-ray scattering

Wide-angle X-ray scattering (WAXS) studies were performed on a Siemens D500 diffractometer employing nickel-filtered CuKα radiation. The 2θ scan rate was 1°/min. Diffractometer scans were run on the as-polymerized 3.2 mm thick plaques in the reflection mode.

Mechanical properties

Mechanical properties were measured according to ASTM D-638 using a screw-driven Instron testing machine. Elongation rate was 50 mm min^{-1}. Three to five tests were made on each sample depending on availability.

Optical microscopy

Samples were microtomed for optical microscopy using an American Optical microtome. Samples were frozen in liquid nitrogen and sectioned with a glass knife. Sections were then examined with a Zeiss polarizing microscope using magnifications of 20 to 400 X.

Adiabatic temperature rise

The adiabatic temperature rise was measured for the 10–77% hard segment series to give an estimate of the possible polymerization conditions encountered in the centre of the mould. A 4% molar excess of moulten MDI at 60°C was added to a degassed mixture of PPO–EO, BDO and catalyst. This mixture was then rapidly stirred for 30 s with a high-speed mechanical mixer. The reacting mixture was quickly poured into a disposable 250 ml beaker with a thermocouple fixed at the centre. The temperature in the centre of the polymerizing mixture was monitored as a function of time. The temperature rise measured was judged to be adiabatic since the maximum temperature was obtained within 3 to 4 min and the rate of temperature decay from the maximum was less than 1°C min^{-1}.

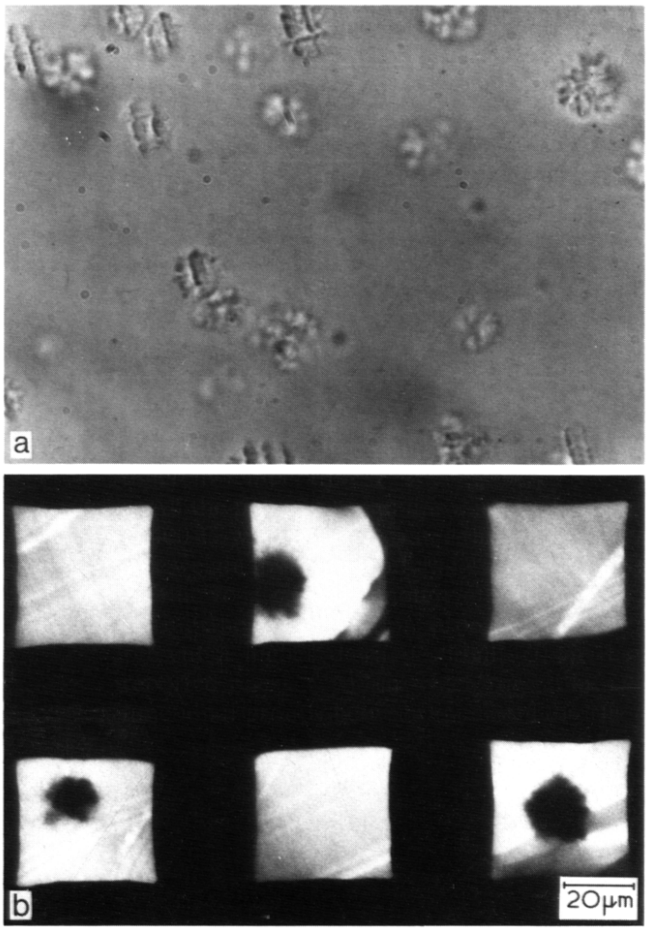

Figure 1 Micrographs of the globular morphology of sample I (10% hard segment, both micrographs same magnification): (a) optical micrograph (uncrossed polarizers); (b) *TEM* micrograph

RESULTS

Optical microscopy

Sample I was found to be isotropic with no birefringent regions or spherulites present. In unpolarized light approximately 10 μm diameter globules were observed (see *Figure 1a*). Microtome knife marks can be seen traversing the globules indicating that the globules have a higher modulus than the surrounding soft segment matrix.

Sample II showed more globules than sample I along with very faint areas of birefringence probably corresponding to very small, poorly formed spherulites.

Sample III was similar to sample IV although there were fewer and smaller spherulites. In sample IV the spherulites were uniformly distributed across the mould although not volume filling (see *Figures 2a* and *9b*). In sample V (55% hard segment) the spherulites are volume filling across the entire mould (see *Figures 2b* and *10b*). There is a slight skin/core variation in sample V with the core appearing less birefringent than the skin. This could be due to a higher concentration of globules at the core or incomplete impingement of the spherulites.

Samples up to 55% hard segment content are uniform in appearance across the mould to the naked eye. The two highest hard segment urethanes, samples VI and VII exhibit a morphology that depends on the position in the mould. Examination of sample VI shows spherulites mainly near the surface with some spherulites present into the core, although they are small and scattered (see *Figure 2c*). In sample VII there are approximately 40 μm diameter spherulites near the surface while the core region appears homogeneous (see *Figures 2d* and *12b*). The spherulite size decreases rapidly at about 0.4 mm from the surface.

Differential scanning calorimetry

Figure 3 shows d.s.c. scans of the samples in the temperature range 330K to 550K. Sample I does not exhibit much evidence of hard segment crystallinity, only a small exothermic region is observed, which is probably due to induced crystallization during the d.s.c. run, followed by a small endothermic area.

Sample II shows several melting transitions beginning at about 420K, followed by a small exotherm and re-melting around 495K.

Samples III and IV have similar transitions to sample II though shifted to higher temperatures. For samples II–IV, increasing the hard segment concentration causes a corresponding increase in the transition peak temperature and crystallinity (heat of fusion).

Sample V has the highest transition temperature range and heat of fusion. Samples VI and VII are similar to one another, both having a pronounced lower temperature transition peak centred at 465K and a second higher temperature doublet at 490 and 500K. The 465K peak is present only in samples VI and VII. In general, the transition peaks shift to higher temperatures with increasing hard segment content, reach a maximum at sample V and remain about the same for samples VI and VII. The total heat of fusion and heat of fusion normalized

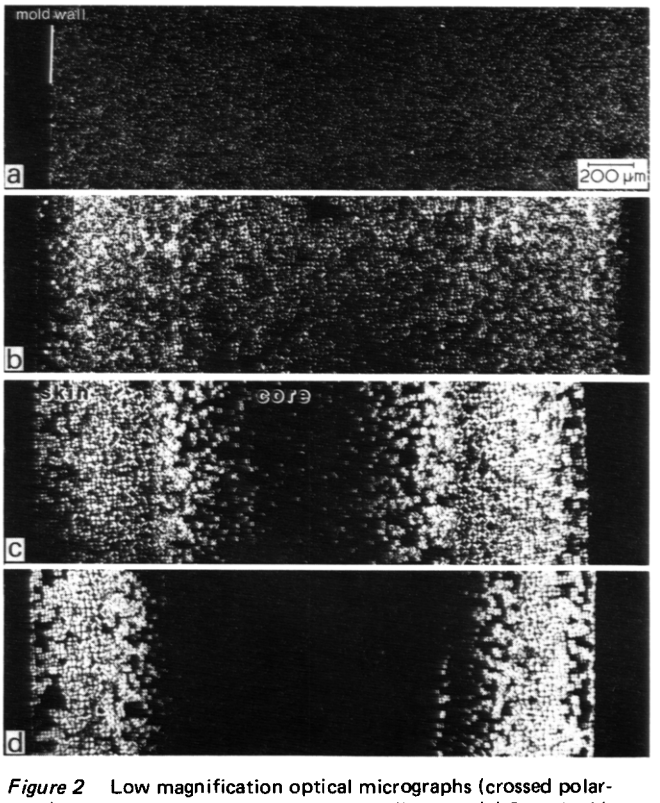

Figure 2 Low magnification optical micrographs (crossed polarizers), all micrographs are the same magnification: (a) Sample IV, 43% hard segment; (b) sample V, 55%; (c) sample VI 66%; (d) sample VII, 77%; note prominent skin/core morphology for (c) and (d); spherulite size increases with increasing hard segment

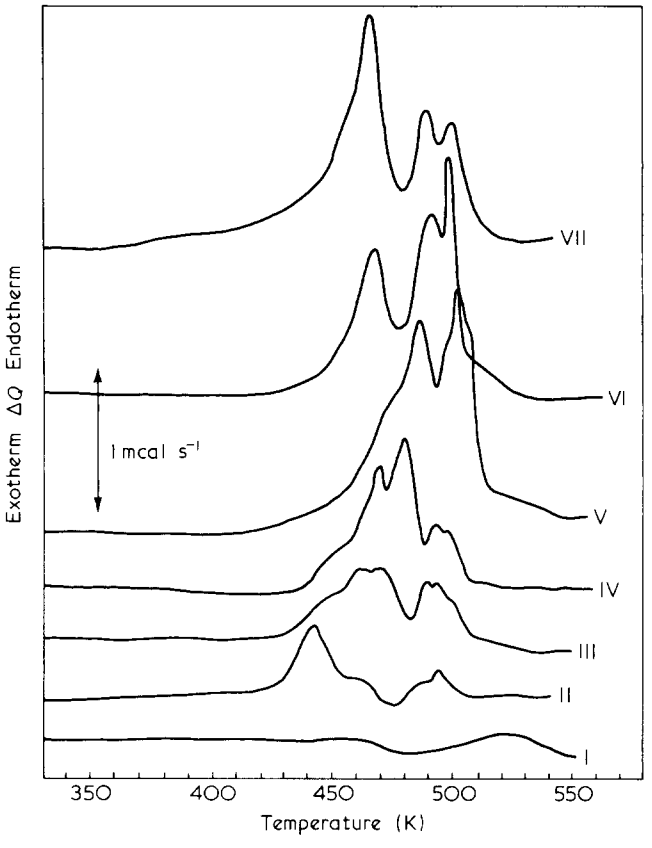

Figure 3 First run d.s.c. scans of samples I–VII over the temperature range 330–550K

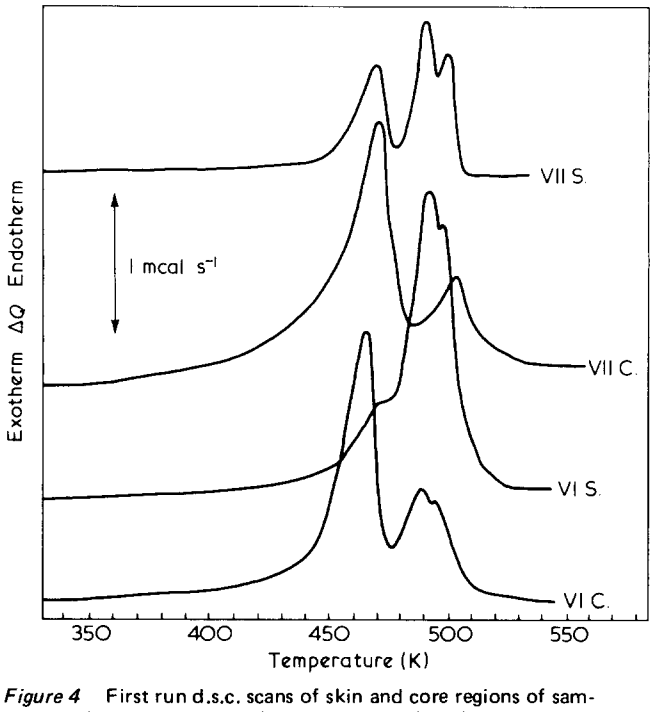

Figure 4 First run d.s.c. scans of skin and core regions of samples VII (77% hard segment) and sample VI (66%). Note the prominent lower temperature peak appearing in the core regions

to sample hard segment content are given in *Table 1*. The heats of fusion per gram of polymer and per gram of hard segment reach a maximum at sample V and then decrease with further increase in hard segment content.

Figure 4 shows d.s.c. scans of the skin and core parts of samples VI and VII. Interestingly, both core portions show a prominent low temperature transition peak (centred at 465K) while skin portions show prominent high temperature transition peaks (centred at 490 and 500K).

Wide-angle X-ray scattering

Wide-angle X-ray scans are shown in *Figure 5*. It is evident from the traces that the highest hard segment content (77%) is not the best organized. The prominent reflections at 4.56 and 3.79 Å are sharpest for sample VI.

Interpretation of the WAXS results must be done carefully for samples VI and VII due to the inhomogeneous distribution of structures present. Calculation of the depth at which the intensity falls to 1/e of the incident intensity indicates that most of the scattering occurs in the top 100 μm of the sample (i.e. in the skin region). The sample which has the highest organization to the depth sampled by WAXS is sample VI.

Mechanical properties

Mechanical properties as determined by stress–strain analysis show a wide range of behaviour, from a soft rubber at low hard segment content through a tough, highly extensible, elastomer at intermediate hard segment concentrations to a higher modulus thermoplastic at high hard segment content (see *Figure 6*). The elongation to break and toughness (measured as the area under the stress–strain curve) shows a maximum at intermediate

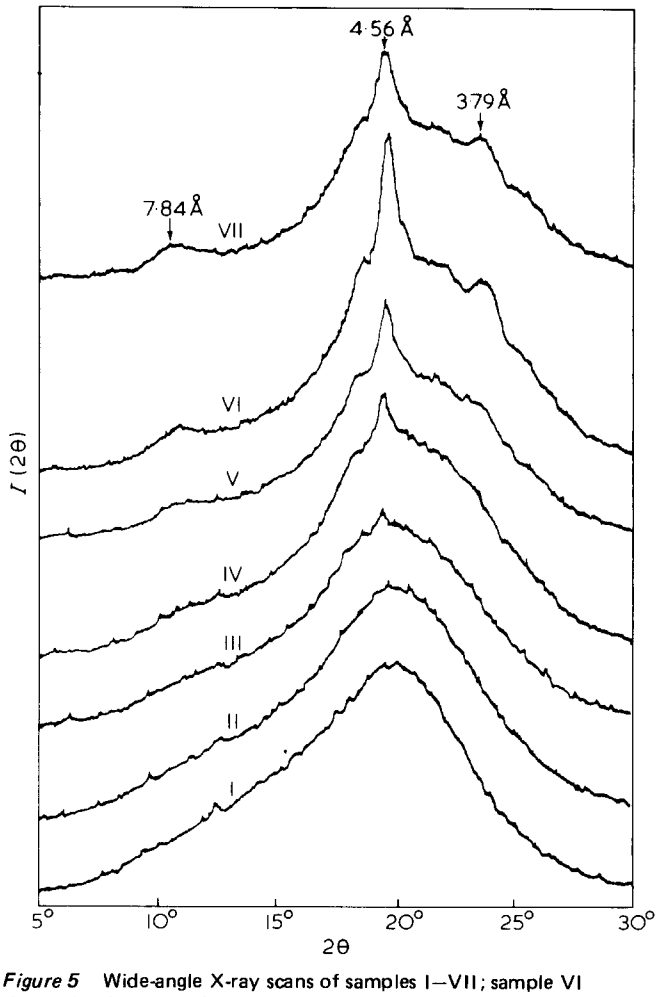

Figure 5 Wide-angle X-ray scans of samples I–VII; sample VI shows the sharpest reflections

hard segment concentrations (see *Table 2*). Zdrahala *et al.*[14] noted an inflection in the tensile strength *versus* hard segment concentration curve for these samples which they interpreted as phase inversion from a soft segment rich matrix to a hard segment rich matrix occurring at about 55% hard segment content.

TEM *results*

Of all the experimental tools presently employed, electron microscopy of microtomed sections is the most localized probe of sample microstructure. *TEM* shows all samples to be heterogeneous at the μm scale and below. Sample I of only 10% hard segment content displays a few widely separated 10μm diameter dark spherical regions, resembling previously observed hard segment globules (*HSG*) (see *Figure 1b*)[13]. Sample II has similar globules though they are larger and more numerous (see *Figure 7*). The globules are embedded in a featureless matrix. Samples III and IV show an increasing volume fraction of similar globules as well as dark, radial, fibrillar hard segment-rich spherulites (*HSS*) in a lighter, featureless soft segment-rich matrix (*SSM*) (see *Figures 8*, *9a* and *9b*).

Sample V (55% hard segment) consists of hard segment-rich spherulites and globules with almost no soft segment matrix (see *Figure 10a*). As mentioned earlier, d.s.c. and optical microscopy indicate a distinct skin/core morphology for samples VI and VII. The surface regions of samples V, VI, and VII display 2 types of volume filling spherulites. The α are smaller, internally diffuse spherulites while type β spherulites appear larger, with a prominent radial fibrillar structure (see *Figures 11a*, *12a* and *12b*). There is a good correlation between optical and electron microscopy for samples IV to VII (see *Figures 9–12*). Still, it is difficult to distinguish between hard-segment-rich globules and type α spherulites with electron microscopy and polarized light microscopy due to the diffuse internal nature of type α spherulites. *Figure 1b* (sample I) clearly shows globules and *Figure 11a* (sample VI) shows α spherulites. At other hard segment concentrations the distinction is not as clear. Undoubtedly, there is a relationship between globules and α spherulites that is not well understood at present.

The core regions of samples VI and VII are quite different from the surface regions. The core of sample VI exhibits a few type β spherulites immersed in a featureless hard-segment-rich matrix (*HSM*) (see *Figure 11b*). The core of sample VII is a continuous hard-segment-rich matrix with no spherulites (see *Figure 12c*). Although no structure was found by optical or electron microscopy, d.s.c. indicates the presence of crystallinity in the core of samples VI and VII. Therefore the crystallite size is small, possibly combined with paracrystalline ordering, causing the imaging of the domains to be difficult.

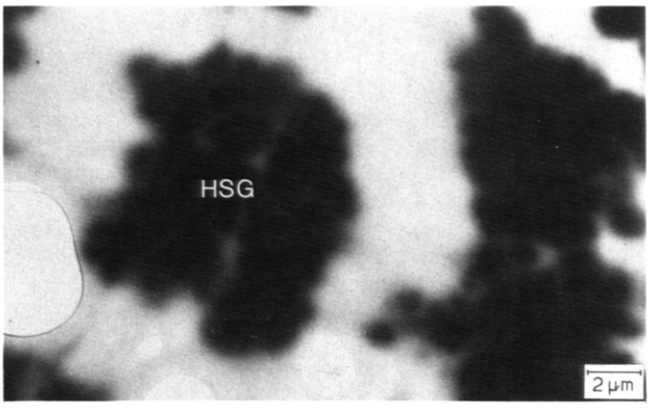

Figure 7 *TEM* micrograph of sample II (21% hard segment). Note the hard segment-rich globules (*HSG*)

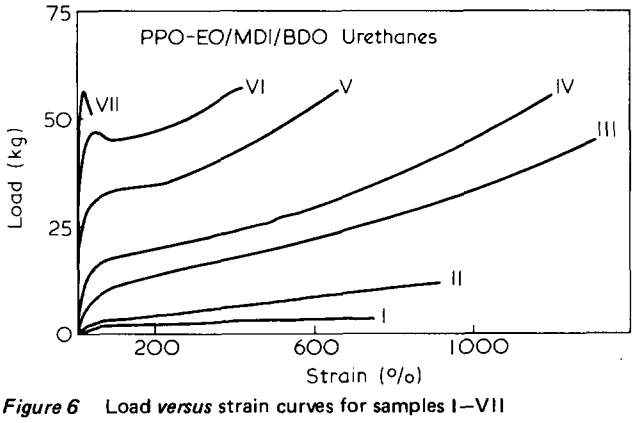

Figure 6 Load *versus* strain curves for samples I–VII

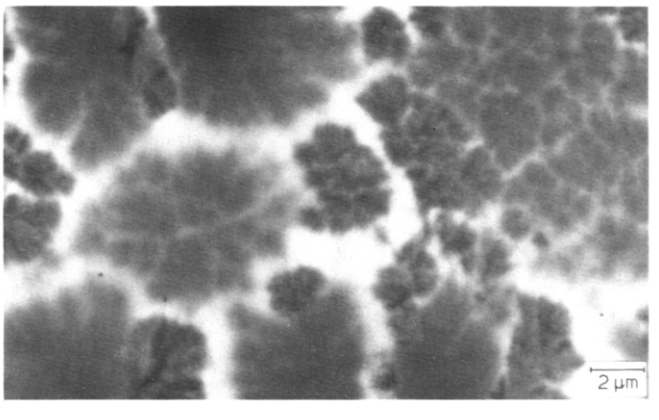

Figure 8 *TEM* micrograph of sample III (32% hard segment)

Table 2 Mechanical properties of PPO–EO/MDI/BDO urethanes

Sample designation	Initial modulus (MPa)	Yield stress (MPa)	Ultimate elongation (%)	Fracture stress (MPa)	Toughness ($J\,m^{-3}$)
I	0.7	–	700	1.7	8.3×10^7
II	5.5	–	800	7.8	3.3×10^8
III	3.4	–	1400	22	2.1×10^9
IV	130	–	1200	33	2.6×10^9
V	260	–	700	31	1.7×10^9
VI	520	30	400	33	1.2×10^9
VII	1400	44	40	38	1.6×10^8

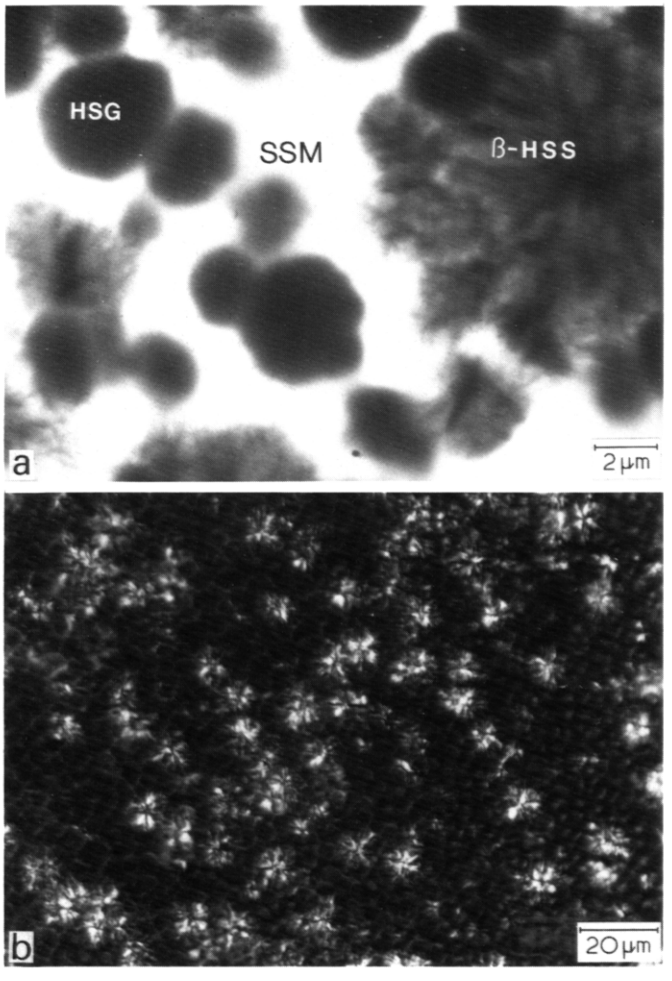

Figure 9 Micrographs of sample IV (43% hard segment), (a) *TEM* micrograph, note the presence of hard segment-rich globules (*HSG*), spherulites (*HSS*) and soft segment-rich matrix (*SSM*); (b) optical micrograph (crossed polarizers)

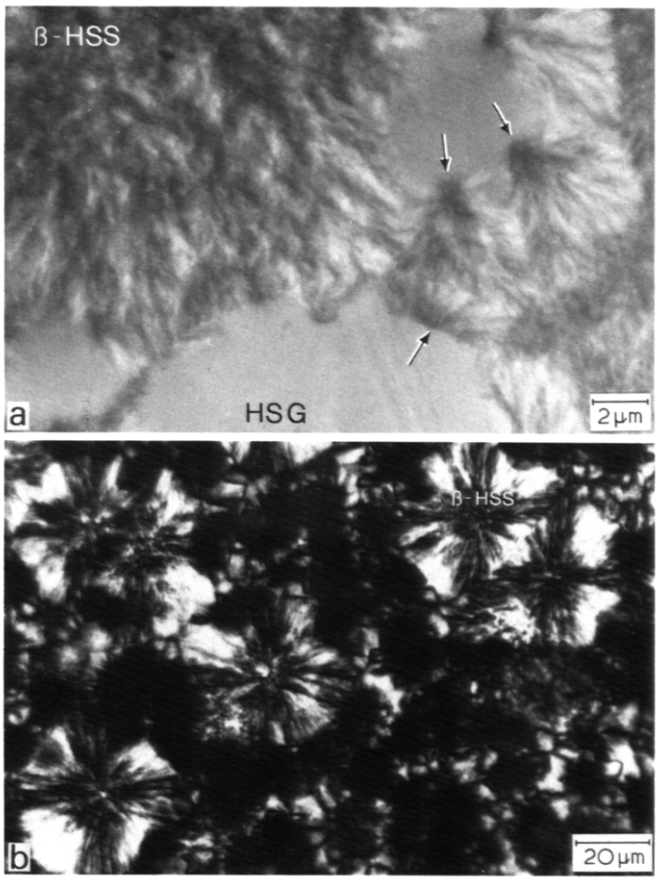

Figure 10 Micrographs of sample V (55% hard segment): (a) *TEM* micrograph showing β spherulites nucleated from hard segment-rich globules, arrows indicate nucleation centres; (b) optical micrograph (crossed polarizers) showing β spherulites and non-birefringent regions

SEM *results*

Figures 13a and *13b* are *SEM* micrographs of the surface of sample VII before and after tensile deformation. The spherulites can be seen in the undeformed material as polyhedral, dimpled surface irregularities. The deformed sample has surface cracks running normal to the applied stress, due to the break up of the spherulitic skin along the spherulite boundaries during deformation while the underlying core material (regions labelled CR) has undergone ductile deformation. It is evident that the skin/core morphology has a profound effect on the mechanical properties of the material.

Adiabatic temperature rise results

Figure 14 is a plot of the maximum temperature attained under adiabatic conditions *versus* hard segment content. The solid line is the calculated temperature rise based on equation (1)*:

$$T_{max} = \frac{\Delta Hc}{\rho C_p} + T_{max} \qquad (1)$$

where $\Delta H = 20000$ cal mol^{-1} OH groups; density, $\rho = 1.14$ g cm^{-3}; specific heat, $C_p = 0.45$ cal g^{-1} K^{-1};

* Values adopted from Ref. 16.

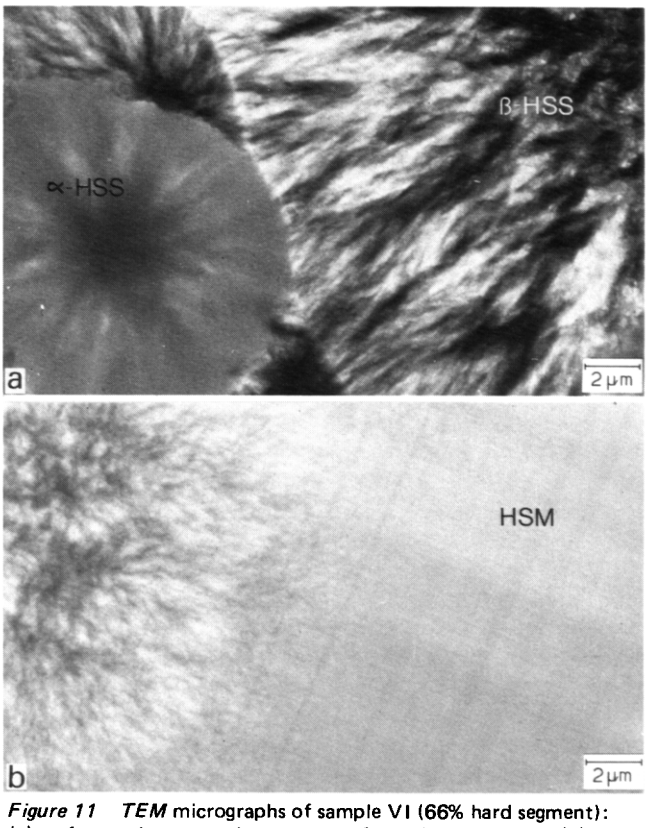

Figure 11 *TEM* micrographs of sample VI (66% hard segment): (a) surface region, note the presence of α and β spherulites; (b) core region with β spherulite surrounded by hard segment-rich matrix (*HSM*)

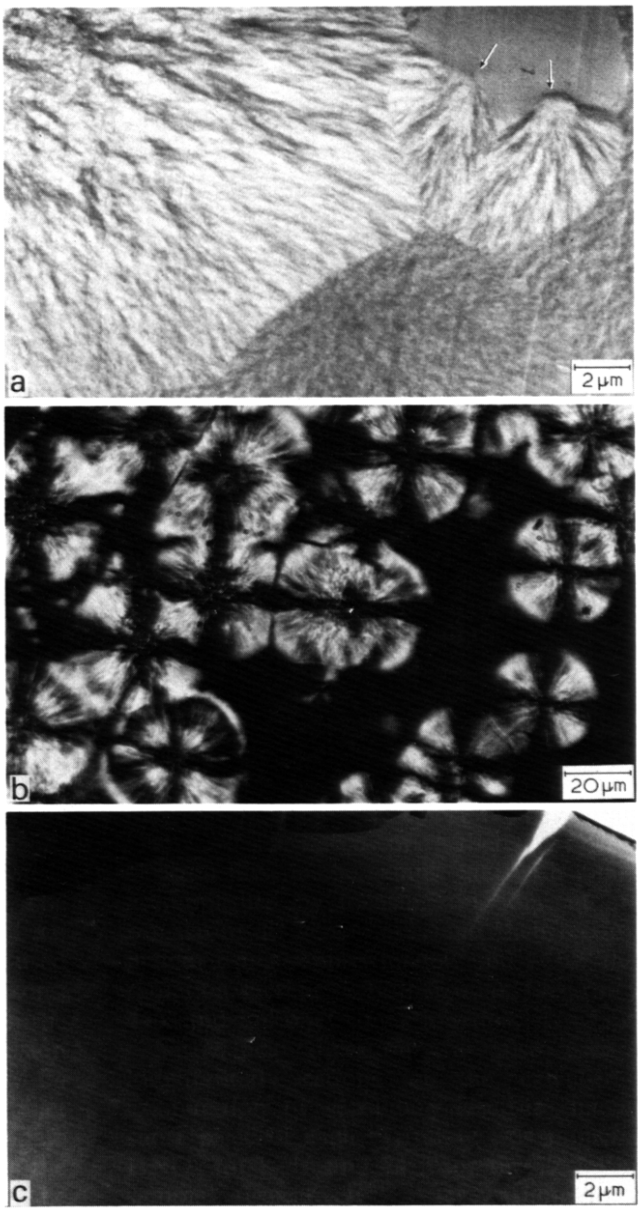

Figure 12 Micrographs of sample VII (77% hard segment): (a) *TEM* micrograph of the surface region showing β spherulites and globules; (b) optical micrograph of surface region (crossed polarizers) showing β spherulites; (c) core region showing homogeneous hard segment-rich matrix. The upper left edge of the microtomed section has folded over

T_{mix} = mix temperature of reactants; c = concentration in moles (OH groups) cm^{-3}.

As expected, the experimental temperature rise values are consistantly less than the calculated values due to factors such as incomplete mixing and heat transfer which limit the maximum temperature attainable. It is noteworthy that for samples VI and VII the maximum temperature rise is well into the melting range of the crystalline hard segment as measured by d.s.c.

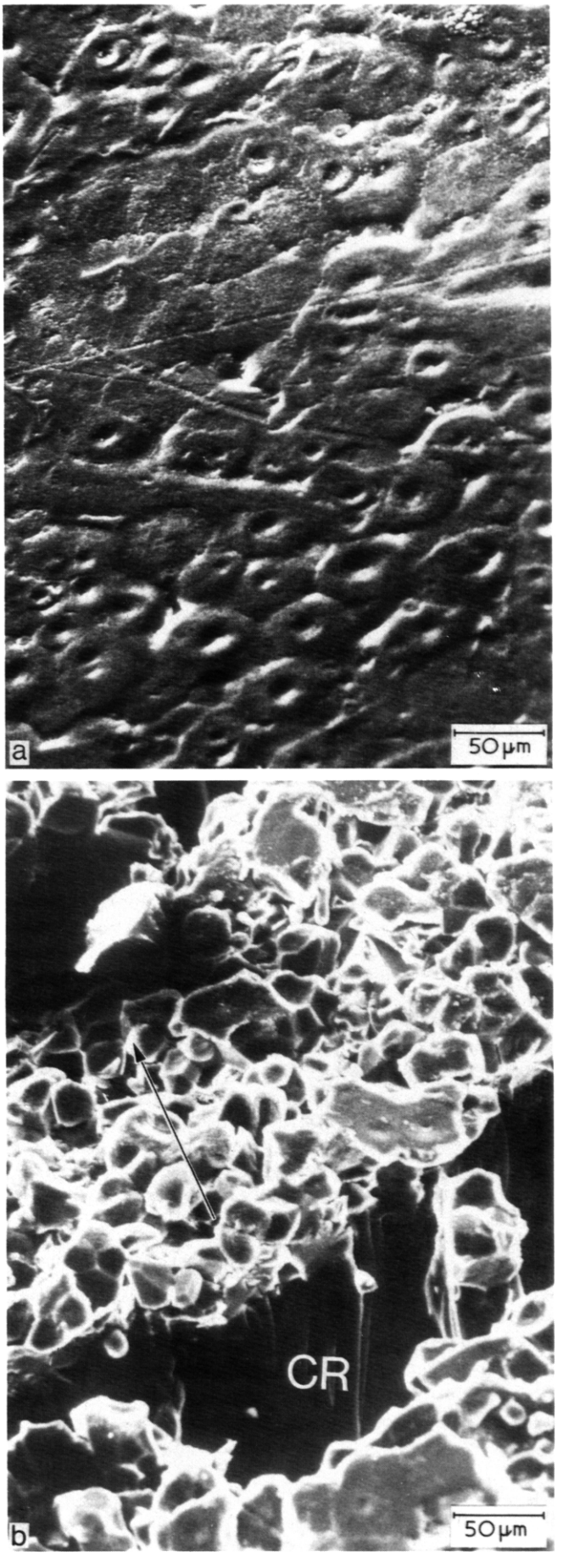

Figure 13 *SEM* micrographs of sample VII: (a) before tensile deformation, the spherulites at the skin are visible as polyhedral, dimpled irregularities on the surface; (b) with tensile deformation, surface cracks appear at spherulite boundaries. The core region (labelled CR) underwent ductile deformation. Deformation direction indicated by the arrow

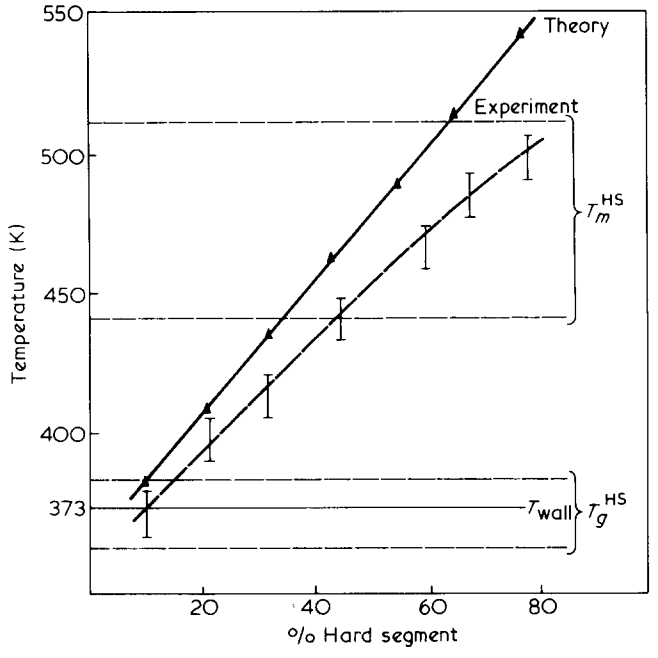

Figure 14 Calculated and experimental adiabatic temperature rise *versus* hard segment content

DISCUSSION

The present study was undertaken to learn more about the origins and nature of the larger scale microstructures previously observed in a *RIM* polyurethane based on polycaprolactone/MDI/BDO of 43 weight per cent hard segment[13]. Their influence on mechanical properties was also investigated. Use of a relatively low catalyst concentration was expected to yield a systematic series of homogeneous urethanes polymerized isothermally at 100°C.

Although skin/core differences in samples VI and VII were found with virtually every characterization method, the techniques do not sample identical regions of the specimen. Moreover, the morphology variation is continuous and the division of the sample into skin and core regions is an oversimplification. Nevertheless, the dramatic skin/core morphology variations found in samples VI and VII and the hard segment-rich globules found even in the lowest hard segment content sample, indicate that the concept of isothermal polymerization from well-mixed components needs closer scrutiny.

Any morphological variations found must be determined within the early stages of polymerization, for after this initial period the temperature histories of the samples are essentially the same. The 10μm scale heterogeneous globule morphology of sample I suggests that the assumption of an initially homogeneous system which undergoes phase-separation during polymerization[17,18] does not hold for this system. In the following discussion, rather than attempting to account in detail for each of the complex sample microstructures, we concentrate on understanding the underlying principles leading to the general types of microstructures observed.

Globules

First, it is important to note that the MDI monomer quickly separates from the diol/polyol mixture at 55°C, the approximate mix temperature of the reactants. Therefore the mixing may produce only a partly-dispersed system with small, moulten MDI-rich droplets in a predominantly polyol/diol-rich matrix at low hard segment concentrations or small polyol/diol-rich droplets in an MDI-rich matrix at high hard segment concentrations (*Table 1* shows the starting volume fraction of each monomer in the mixture).

Secondly, since large round thickness variations over a scale of 1 to 10 μm within a microtomed section are extremely unlikely, the strong contrast seen in bright field *TEM* must be due to electron density variations caused by compositional changes. The dark, electron dense, globules observed at low hard segment concentrations are therefore MDI-rich regions. To form such globules in the low MDI content samples through phase separation and coalescing of hard segments from an initially homogeneous system, diffusion would have to occur over many tens of μm in a matter of minutes, which is hardly feasible for high molecular weight polymers.

The appearance of globules is also dependent on sample composition. The volume fraction of globules increases with hard segment (MDI) content up to sample V, then sharply decreases with a concomitant increase in the two types of hard segment-rich spherulites. Such a morphology could arise from MDI becoming the continuous phase in combination with the high temperatures and high mobility during the polymerization caused by the large exotherm. These conditions would disperse any PPO–EO droplets formed initially, and promote hard segment crystallization.

This type of morphology is probably characteristic of reaction-moulded systems with incompatible components. The two-phase 'nodular' or 'microgel' morphology seen in many epoxy systems could be due to a similar mechanism[19–21].

Spherulites

The two types of hard segment spherulites have different nucleation and growth characteristics. Type α spherulites appear to nucleate first but then grow slowly. At sufficient undercooling type β spherulites nucleate, often at the growth front of type α spherulites or globules (see arrows in *Figures 10* and *12a*), and have a much faster growth rate reaching a larger average size and volume fraction.

The adiabatic temperature rise results show that the exothermic heat of reaction causes a substantial temperature rise in the (adiabatic) core. These results are probably a good estimate of the reaction conditions found at the core of the mould. As the urethane reaction proceeds, the sample temperature rises, mainly due to the heat of reaction, and somewhat due to heat input from the 100°C mould wall. Once the skin region is above 100°C the mould wall will conduct heat away from the surface of the sample reducing the temperature rise in the skin region. Time–temperature plots as a function of mould position have been calculated by Macosko and coworkers for bulk polyurethane reactions[16,22]. Generally they take the shape as in *Figure 15* with a steep, rapid rise from the reactant mix temperature to a maximum, followed by a slow decay to the mould temperature. The large amount of heat liberated with the 66% and 77% hard segment samples brings the temperature at the core within the melting range of the hard segment and into the relatively slow, nucleation controlled crystallization regime (see *Figure 15a*). The crystallization in the core region of

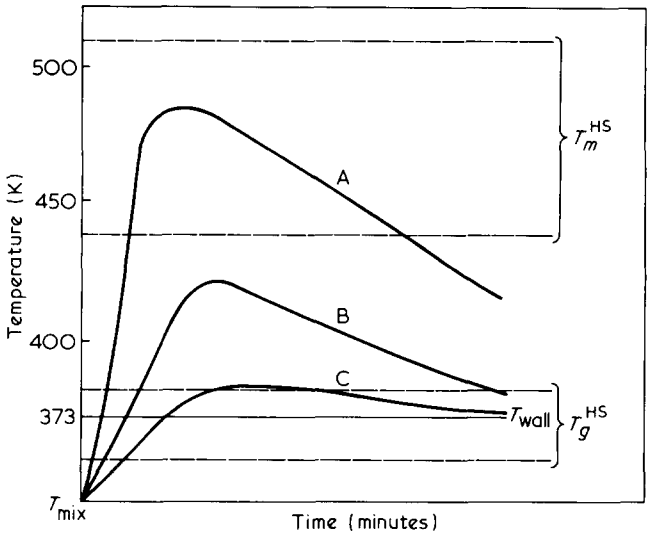

Figure 15 Possible temperature *versus* time pathways for different compositions: (A) high hard segment content; (B) intermediate hard segment content; (C) low hard segment content

samples VI and VII probably resembles conventional crystallization after cooling from the melt. In the skin of samples VI and VII heat conduction to the wall limits the temperature rise and the crystallization kinetics are faster promoting the development of well-formed β spherulites (see *Figure 15b*). At lower hard segment concentrations (samples IV and V) the temperature rise is less and the sample morphology becomes more uniform with well-formed β spherulites throughout the specimen (see *Figure 15b*). This also explains the variation of crystallinity with hard segment concentration seen by d.s.c. and WAXS. With sample V, a balance is struck between mobility, molecular weight and crystallization kinetics, yielding the highest crystallinity (total area of all d.s.c. peaks). At the lower hard segment concentrations, the size and number of spherulites decrease due to the lower temperature rise and the crystallization kinetics becoming diffusion-controlled (see *Figure 15c*). In addition, there is less hard segment of sufficient sequence length to crystallize.

As mentioned previously both toughness and ultimate elongation reach a maximum at intermediate hard segment concentrations where there is a corresponding maximum in the product of the volume fractions of the two phases. The mechanical properties are a composite average of the influence of hard segment globules, spherulites and soft or hard segment matrix material and although informative, certainly do not represent the full potential possible for urethanes over this composition range.

CONCLUSIONS

In summary, the morphology of reaction-moulded systems with incompatible starting components depends on composition, degree of mixing, mobility of components and temperature history. In addition, the detailed sample temperature history depends on position in the mould due to the large exothermic heat of reaction and heat transfer with the mould walls. For low hard segment content polyurethanes, the mould temperature gradient will be small, whereas for high hard segment content materials, temperature gradients of 100°C or more can occur. The important part of the reaction, during which the μm and the 100 Å scale morphology is determined, is the first few minutes (seconds for *RIM* formulations) before the solidification of the mixture. The complex, simultaneously occurring (macro)phase separation–polymerization–(micro)phase separation–crystallization processes will vary according to sample composition, position in the mould and the detailed temperature history. While a phase inversion from a soft segment-rich matrix to a hard segment-rich matrix does occur between samples IV and V, interpreting the relationship between mechanical properties and microstructure is greatly complicated by the influence of the variations and heterogeneties present in the morphology.

ACKNOWLEDGEMENT

Acknowledgement is made to the National Science Foundation, Grant DMR79-09726, Polymers Program (Industrial–Academic Program) and to Union Carbide, Chemicals and Plastics, South Charlestown, West Virginia, for financial support. The use of the facilities of the Materials Research Laboratory at the University of Massachusetts is gratefully acknowledged. The authors are also pleased to acknowledge helpful discussions with Professor C. W. Macosko of the University of Minnesota.

REFERENCES

1 Allport, D. C. and Mohajer, A. A. 'Block Copolymers, (Eds. D. C. Allport and W. H. Janes), Appl. Sci. Pub., 1973, p 443
2 Manson, J. A. and Sperling, L. H. 'Polymer Blends and Composites', Plenum Press, 1976, p 153
3 Noshay, A. and McGrath, J. E. 'Block Copolymers', Academic Press, 1977, p 370
4 Huh, D. S. and Cooper, S. L. *Polym. Eng. Sci.* 1971, **11**, 369
5 Ferguson, J. and Ahmad, N. *Eur. Polym. J.* 1977, **13**, 865
6 Lagasse, R. R. *J. Appl. Polym. Sci.* 1977, **21**, 2489
7 Lunardon, G., Sumida, Y. and Vogl, O. *Angew. Makromol. Chem.* 1980, **87**, 1
8 Kimura, I., Ishihara, H., Ono, H., Yoshihara, N., Nomura, S. and Kawai, H. *Macromolecules* 1974, **7**, 355
9 Samuels, S. L. and Wilkes, G. L. *J. Polym. Sci., Polym. Symp.* 1975, **43**, 149
10 Seymour, R. W., Overton, J. R. and Corley, L. S. *Macromolecules* 1975, **8**, 331
11 Wilkes, G. L., Samuels, S. L. and Crystal, R. *J. Macromol. Sci., Polym. Phys. Edn.* 1974, **10**, 203
12 Schneider, N. S., Desper, C. R., Illinger, J. L., King, A. O. and Barr, D. R. *J. Macromol. Sci. (B)* 1975, **11**, 527
13 Fridman, I. D., Thomas, E. L., Lee, L. J. and Macosko, C. W. *Polymer* 1980, **21**, 393
14 Zdrahala, R. J., Gerkin, R. M., Hater, S. J. and Critchfield, F. E. *J. Appl. Polym. Sci.* 1979, **24**, 2041
15 Fridman, I. D. *Master's Thesis*, University of Massachusetts (September 1979)
16 Castro, J. M. and Macosko, C. W. *AIChE J.* 1982, **22**, 11
17 Tirrell, M., Lee, L. J. and Macosko, C. W. *ACS Symp. Ser.* 1979, **104**, 149
18 Castro, J. M., Lopez-Serrano, F., Carmargo, R. E., Tirrell, M. and Macosko, C. W. *J. Appl. Polym. Sci.* 1981, **26**, 2067
19 Misra, S. C., Manson, J. A. and Sperling, L. H. *ACS Symp. Ser.* 1979, **114**, 157
20 Mijovic, J. and Koutsky, J. A. *Polymer* 1979, **20**, 1095
21 Cuthrell, R. E. *J. Appl. Polym. Sci.* 1967, **11**, 949
22 Lee, L. J. and Macosko, C. W. *Soc. Plast. Eng. Tech. Papers* **24**, 155